Electronic Supplementary Material (ESI) for ChemComm.
This journal is © The Royal Society of Chemistry 2019

Supporting Information

Anisotropic elasticity and plasticity of organic crystal

Jian-Rong Wang, Meiqi Li, Qihui Yu, Zaiyong Zhang, Bingqing Zhu, Wenming Qin, and Xuefeng Mei**

EXPERIMENTAL SECTION:

Materials. Vitamin D_3 (**A**) and cholesterol were obtained from Zhejiang Garden Biochemical High-Tech Co., LTD. Vitamin D_2 (**C**), *trans*-4-tert-butylcyclohexanol (**D**), and *cis*-4-tert-butylcyclohexanol (**E**) were obtained from J&K Chemical Ltd, with greater than 99% purity. All analytical grade solvents were purchased from Sinopharm Chemical Reagent Co., Ltd and used without further purification.

Synthesis of 3α-cholesterol (B). A mixture of cholesterol (2 g), triphenylphosphine (2.03 g) and 4-nitrobenzoic acid (1.03 g) was dissolved in THF (20 mL) and cooled to −5 °C. The diethylazodicarboxylate (1.21 mL) was added dropwise to the mixture and keep the reaction at -5 °C for 5 min. Allowing the reaction stirring at room temperature for 12 h and then quenched with saturated NH_4Cl solution (20 mL). Extracted with DCM twice (20 ml × 2), combined the organic solvent and washed with water (20 mL). Then dried with anhydrous $MgSO_4$, filtered and concentrated under reduced pressure to get the crude intermediate as white solid. The crude intermediate was dissolved in MeOH/H_2O (4:1, 20 mL) and LiOH·H_2O (1.08 g) was added. The reaction was stirring at room temperature for 12 h and diluted with H_2O (20 mL), extracted with EtOAc (20 mL × 2). The organic extract was dried, filtered, concentrated and the residue was purified by silica gel chromatography (ethyl acetate/hexane, 1:4), affording 520 mg of **B** (27%).

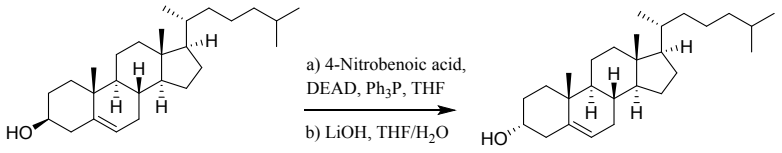

cholesterol 3α-cholesterol

Preparation of AB_2. A mixture of **A** (7.7 mg, 0.02 mmol) and **B** (15.4 mg, 0.04 mmol) was dissolved in 1 mL methanol by heating. The addition of 4 mg of VB_9 and cooling down to room temperature resulted in the immediate formation of gels, and then kept in 4 °C. Crystals grew within a few days. The gels are then dissolved by addition of 10 μL Et_3N. The colorless needle-shaped crystals of $\mathbf{AB_2}$ were recovered by filtration.

Preparation of BC_2. A mixture of **B** (7.7 mg, 0.02 mmol) and **C** (15.8 mg, 0.04 mmol) was dissolved in 1 mL methanol by heating. The addition of 4 mg of VB_9 and cooling down to room temperature resulted in the immediate formation of gels, and then kept in 4 °C. Crystals grew within a few days. The gels are then dissolved by addition of 10 μL Et_3N. The colorless needle-shaped crystals of $\mathbf{BC_2}$ were recovered by filtration.

Preparation of DE_2. A mixture of **D** (46.8 mg, 0.3 mmol) and **E** (93.6 mg, 0.6 mmol) was dissolved in 1 mL dimethyl sulfoxide / nitromethane (2:8). The addition of 6 mg of VB_9 and cooling down to room

temperature resulted in the immediate formation of gels, and then kept in 4 °C. Crystals grew within a few days. The gels are then dissolved by addition of 10 μL Et_3N. The colorless needle-shaped crystals of **DE**$_2$ were recovered by filtration.

Scanning electron microscopy (SEM). SEM analysis was carried out with a QUANTA FEG 450 electron microscope with a primary electron energy of 2–5 kV at room temperature. The crystals were attached to silicon wafers with oil or adhesive.

Powder X-ray diffraction (PXRD). PXRD patterns were obtained using a Bruker D8 Advance X-ray diffractometer (Cu Kα radiation). Voltage and current of the generator was set to 40 kV and 40 mA, respectively. Data over the range 3−40° 2θ were collected with a scan rate of 5°/min at ambient temperature. The data were imaged and integrated with RINT Rapid and peaks were analyzed with Jade 6.0 from Rigaku. Calibration of the instrument was performed using a corindon standard (Bruker AXS Korund-probe).

Single-crystal X-ray diffraction (SCXRD). X-ray diffractions of all single crystals were carried out at 170(2) K on a Bruker Apex II CCD diffractometer using Mo Kα radiation (λ = 0.71073 Å). Integration and scaling of intensity data was performed using the SAINT program. Data were corrected for the effects of absorption using SADABS. The structures were solved by direct method and refined with full-matrix least-squares technique using SHELX-2014 software. Non-hydrogen atoms were refined with anisotropic displacement parameters, and hydrogen atoms were placed in calculated positions and refined with a riding model. Crystallographic data in cif format have been deposited in the Cambridge Crystallographic Data Center, CCDC No. 1879755-1879757, respectively. Crystallographic data and refinement details are summarized in Table S1.

Thermogravimetric analysis (TGA). Thermogravimetric analysis was carried out on Netzsch TG 209F3 equipment. Samples were placed in open aluminum oxide pans and heated at 10 °C min^{-1} to 400 °C. Nitrogen was used as purge gas at 20 mL min^{-1}.

Differential scanning calorimetry (DSC). DSC experiments were performed on a DSC TA Q2000 instrument under a nitrogen gas flow of 50 mL·min^{-1} purge. Ground samples weighing 1−3 mg were heated in sealed aluminum pans at a heating rate 10 °C·min^{-1}. Two-point calibration using indium and tin was carried out to check the temperature axis and heat flow of the equipment.

Synchrotron X-ray studies. Synchrotron crystal diffraction data were collected at the Shanghai Synchrotron MX beamline BL19U1. All the measurements were performed at 100(2) K and with the wavelength λ = 0.9789 Å. All data collections were performed at the BL19U1 beamline with a beam cross-section (full-width at half-maximum (FWHM)) of 50 by 50 μm using an aperture. Data acquisition was performed using Blu-Ice. Data were collected with Pilatus 3-6M detector.

The reversible elastic bending was observed when stress was applied perpendicularly to spring-like backbones on the (100)/(-100) face. Application of stress on the (001)/(00-1) face, in the direction where sliding of layers dominates the packing, leads to plasticity. To determine the structural mechanism that permits this anisotropic flexibility, synchrotron X-ray diffraction was employed. In line with recent reported method,[1] we attempted to probe the structural changes occurring in the bent regions. However, the diffraction pattern from the plastically or elastically deformed regions of the crystals showed significantly broadened (Fig. S3) Bragg peaks that could not be indexed, indicating loss of mono-crystallinity during the event. Especially for plastic bending, layers appear on the striated surface in the bent region in scanning electron microscopy (SEM) images. Although specific structures from the convex to concave sides of the bent section were not obtained, ten conjoint sets of crystallography data near the plastic flexure were collected. The distortion of the unit cell was observed (Table S2), where mainly reflected in the decrease trends of *c* axis and cell volume. Five crystal structures of position 1-5 were successfully solved, which present almost identified crystal parameters, but subtly continuous decrease of *c* axis in unit cell was distinct. This observation implies a gradient of molecular orientations in the bent region. Further analysis of the detailed structure was conducted and molecules in asymmetric unit were compared. The main conformational difference is located at the alkyl side chain. Terminal isopropyl of **A** becomes shrinked when near the flexure, which can be contributed to the sidechain of **A** inserting into the void when plastic bending along *c* axis.

Crystal bending. A pair of tweezers with a straight needle tip were used to hold the crystal from one side while the force was applied on the crystals by a metal needle from the opposite side. Prior application of the mechanical force, the crystals were immersed in oil. All bending experiments were carried out using an Olympus SZ61 Digital Microscope, and the recordings were taken and processed using S-EYE software ver. 1.4.7.543.

Thickness (t) of the crystals were measured prior bending, while the length (L) and maximal displacement (h_{max}) were measured at the point of maximal curvature, just before the crystal fracture.

Radius of the curvature (R) was calculated from the geometric construction given as follows:

$$R^2 = (R - h_{max})^2 + (L/2)^2$$

$$R = \frac{{h_{max}}^2 + L^2/4}{2h_{max}}$$

Bending strain was calculated using the Euler-Bernoulli equation[4] (considering pure bending, *i.e.* bending without shear component):

$$\varepsilon\,(\%) = \frac{t/2}{R} \cdot 100$$

The extent of bending was quantified by calculating bending strains (ε).[2] These experiments, which were carried out on crystals from four different batches of each cocrystal, were highly reproducible and resulted in distinctive and readily identifiable responses. **AB**$_2$ displayed the most pronounced elastic bending (ε = 1.76%) on (100)/(-100) face. For **BC**$_2$ and **DE**$_2$, no perceptible difference in elasticity was observed when the crystals were bent over two major pairs of faces, and they can thus be categorized as 2D elastic crystals. The bending strains are 1.26% and 0.95% for **BC**$_2$ and **DE**$_2$, respectively. Bending strains of three cocrystals are significantly higher than the maximum elastic strain (~ 0.5%) of most crystalline materials.[3] This is attributed to their common feature of helical O-H···O hydrogen bonds, which are fortified by a large number of relatively weak vdW interactions between helix. Notably, **DE**$_2$ presents lower elasticity than that of **AB**$_2$ or **BC**$_2$, indicating the importance of the alkyl chain with a multitude of weak and dispersive interactions in flexible crystals. The different of elasticity (ε value) demonstrates that the nature and extent of elastic bending in crystalline cyclohexanol compounds can be controlled by altering the substituent group in the structure. Importantly, both threefold helical structure and slip plane could be a critical feature that needs to be targeted when attempting to engineer new bendable materials with anisotropic elasticity and plasticity.

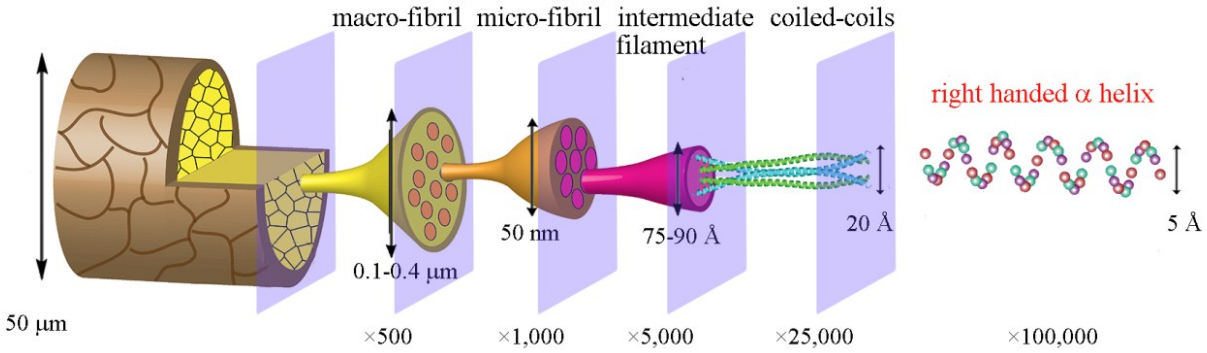

Fig. S1 Elasticity of hair based on its α helical protein.

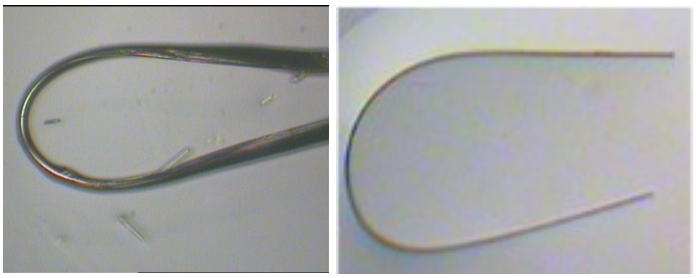

Fig. S2 Plastic bending of AB_2 crystals with a hairpin shape.

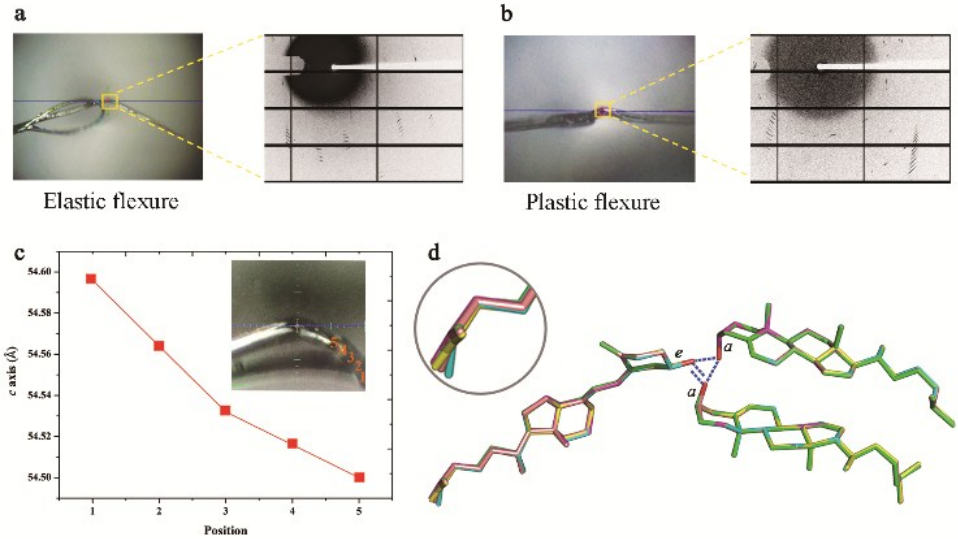

Fig. S3 Structure changes in AB_2 during flexure. (a) Elastic flexure. (b) Plastic flexure. The Bragg peaks from the bent part are significantly broadened. (c) Changes of c axis from the straight part to bent part. (d) Overlay of asymmetric units in five crystal structures.

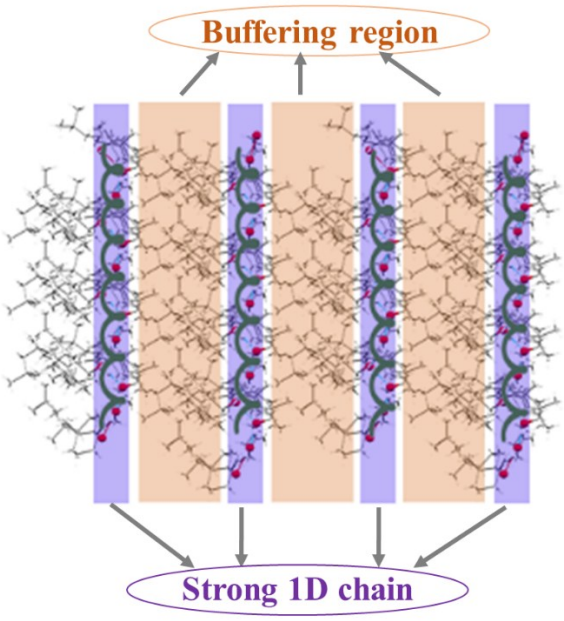

Fig. S4 Elastic crystal face with alternative rigid and buffering regions.

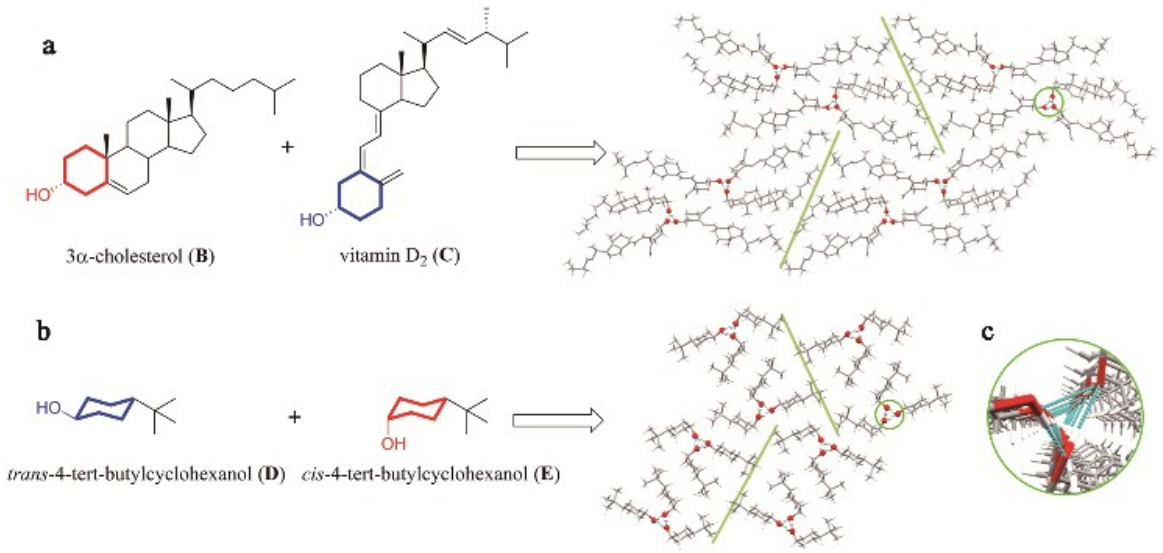

Fig. S5 Crystal structures of **BC**$_2$ and **DE**$_2$. (a) Complementary of a-OH / e-OH synthon to form threefold helix in **BC**$_2$. No slip plane is observed in the crystal. (b) A pair of synthetical cyclohexanol derivatives were designed to form threefold helix. (c) Amplified threefold helix in the crystal structure.

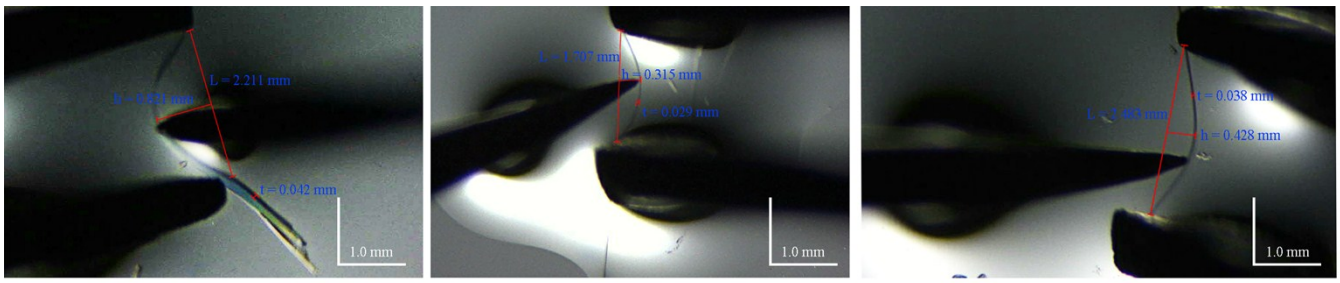

(a) (b) (c)

Fig. S6 Critical bending experiment with $\mathbf{AB}_2$, $\mathbf{BC}_2$, and $\mathbf{DE}_2$.

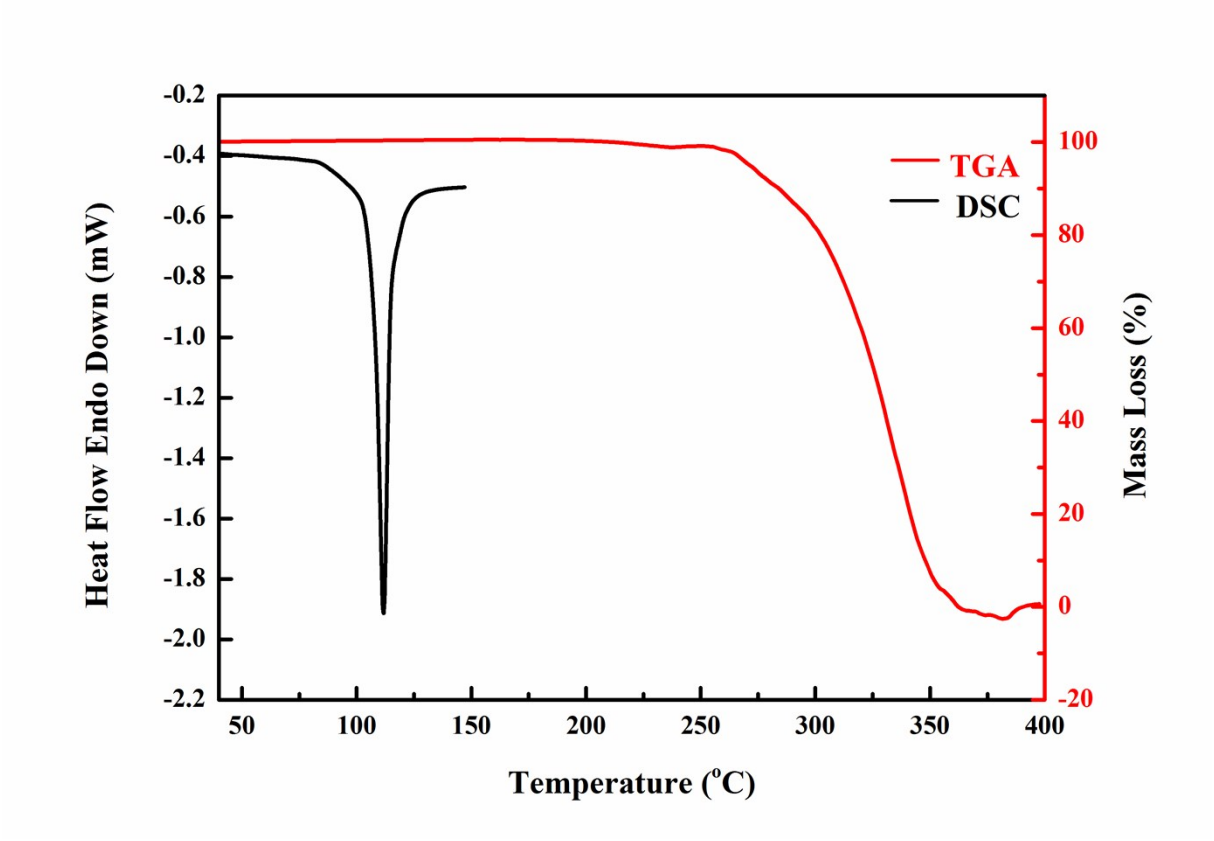

Fig. S5 Thermal analysis of cocrystal $\mathbf{AB}_2$

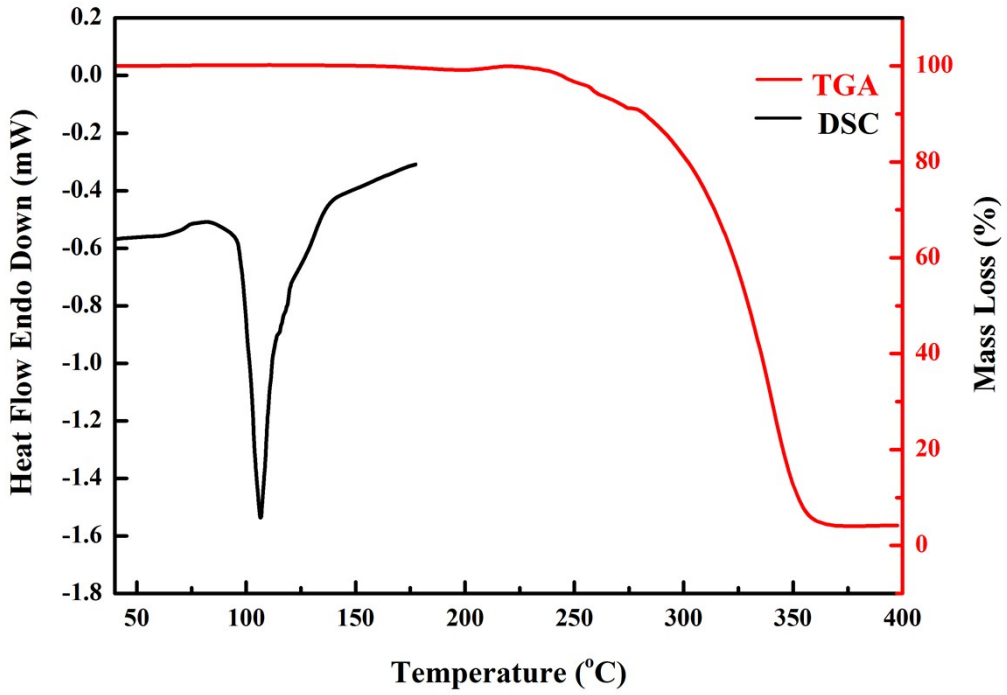

Fig. S6 Thermal analysis of cocrystal **BC**$_2$

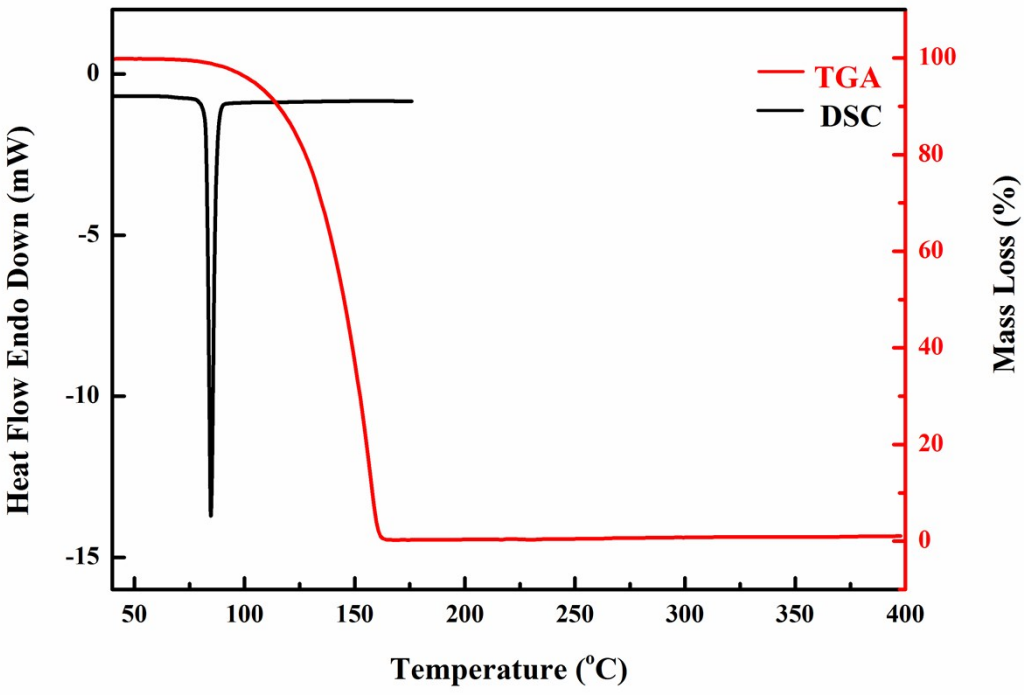

Fig. S7 Thermal analysis of **DE**$_2$

Table S1 Crystallographic Data for cocrystals.

	AB_2	**BC_2**	**DE_2**
Formula	$C_{81}H_{136}O_3$	$C_{83}H_{134}O_3$	$C_{30}H_{60}O_3$
Formula weight	1157.89	1179.89	468.78
Crystal system	Monoclinic	Orthorhombic	Monoclinic
Space group	*C*2	$P2_12_12_1$	$P2_1$/n
Temperature (K)	173(2)	173(2)	173(2)
a (Å)	23.6899(9)	6.4109(3)	6.3307(14)
b (Å)	6.3426(2)	33.5378(14)	29.143(6)
c (Å)	54.772(2)	35.2624(14)	16.376(3)
α (°)	90	90	90
β (°)	95.942(2)	90	98.228(5)
γ (°)	90	90	90
Cell volume (Å^3)	8185.6(5)	7581.7(6)	2990.2(10)
Calc. density (g/cm^3)	0.940	1.034	1.041
Z^a	4	4	4
Z'	1	1	1
λ	1.54178	0.71073	0.71073
S	1.074	1.020	0.970
R_1	0.098	0.066	0.058
R_{int}	0.036	0.071	0.101
wR_2	0.242	0.191	0.151

[a] *Z* represents the number of cocrystal formula in a unit cell

Table S2 Crystallographic Data position 1-10 near the $\mathbf{AB_2}$ plastic flexure for at 100 K.

No.	1	2	3	4	5	6	7	8	9	10
a (Å)	23.616(5)	23.635(5)	23.626(5)	23.612(5)	23.625(5)	23.623(5)	23.646(5)	23.511(5)	23.512(5)	23.449(5)
b (Å)	6.3040(13)	6.3130(13)	6.3140(13)	6.3020(13)	6.3030(13)	6.3160(13)	6.3080(13)	6.2850(13)	6.2930(13)	6.3120(13)
c (Å)	54.596(11)	54.564(11)	54.532(11)	54.516(11)	54.500(11)	54.450(11)	54.403(11)	54.267(11)	54.276(11)	54.076(11)
α (°)	90	90	90	90	90	90	90	90	90	90
β (°)	96.21(3)	96.13(3)	96.17(3)	96.16(3)	96.13(3)	96.15(3)	96.09(3)	96.14(3)	96.14(3)	94.70(3)
γ (°)	90	90	90	90	90	90	90	90	90	90
Cell volume (Å^3)	8080(3)	8095(3)	8088(3)	8065(3)	8069(3)	8060(3)	8071(3)	7972(3)	7982(3)	7942(3)

Note: from position 1 to 10 means more and more near the flexure.

Table S3. Geometrical parameters used to calculate banding strain (ε). The mean values of the bending strain (shown in red) were determined on the basis of measurements of four different samples.

AB_2	t / mm	L / mm	h / mm	R / mm	ε / %
1	0.042	2.211	0.821	1.155	1.82
2	0.029	1.592	0.628	0.818	1.77
3	0.035	2.053	0.776	1.067	1.64
4	0.049	1.581	0.258	1.340	1.83
					1.76

BC_2	t / mm	L / mm		R / mm	ε / %
1	0.029	1.707	0.315	1.314	1.10
2	0.019	1.442	0.424	0.825	1.15
3	0.022	1.236	0.327	0.747	1.47
4	0.033	2.154	0.621	1.244	1.33
					1.26

DE_2	t / mm	L / mm		R / mm	ε / %
1	0.038	2.483	0.428	2.015	0.94
2	0.036	2.125	0.356	1.763	1.02
3	0.029	2.027	0.344	1.665	0.87
4	0.031	1.944	0.329	1.600	0.97
					0.95

References

1 A. Worthy, A. Grosjean, M. C. Pfrunder, Y. Xu, C. Yan, G. Edwards, J. K. Clegg and J. C. McMurtrie, *Nat. Chem.* 2018, **10**, 65-69.

2 M. Dakovic, M. Borovina, M. Pisacic, C. B. Aakeroy, Z. Soldin, B. M. Kukovec and I. Kodrin, *Angew. Chem. Int. Ed.* 2018, **57**, 14801-14805.

3 M. Telford, *Mater. Today* 2004, **7**, 36-43.